Journal of Catalysis 313 (2014) 70–79

Contents lists available at ScienceDirect

Journal of Catalysis

journal homepage: www.elsevier.com/locate/jcat

Biomass conversion to diesel via the etherification of furanyl alcohols catalyzed by Amberlyst-15

Eric R. Sacia, Madhesan Balakrishnan, Alexis T. Bell *

Department of Chemical and Biomolecular Engineering, University of California, Berkeley, 107 Gilman Hall, Berkeley, CA 94720, USA

ARTICLE INFO

Article history:
Received 17 December 2013
Revised 16 February 2014
Accepted 25 February 2014

Keywords:
Furanyl alcohols
Etherification
Biofuels
Diesel
Amberlyst-15
HMF

ABSTRACT

The etherification of furanyl alcohols produced from biomass-derived glucose and fructose has been a growing area of research for production of alternative diesel additives. We have determined that the Brønsted acidic resin catalyst, Amberlyst-15, is highly active and selective for the etherification of furanyl alcohols by both ethanol and butanol. The mechanism and kinetics of this reaction were investigated using 5-methylfurfuryl alcohol (MFA) as a probe molecule. Etherification of MFA was found to be first order in both the concentrations of furanyl alcohol and the acid sites. The mechanism of MFA etherification also holds for the etherification of 2,5-bis(hydroxymethyl)furan (BHMF) and 5-(hydroxymethyl)furfural (HMF). In the case of HMF, we find that acetalization of HMF precedes etherification in alcohol solutions. The apparent activation energy of furanyl alcohol etherification in ethanol and butanol solutions ranged from 17.0 to 26.3 kcal/mol. Electron donation/withdrawal at the 2 or 5 position of the furan ring in addition to solvent polarity was found to have significant effects on the rate of furanyl alcohol etherification.

1. Introduction

Both the European Union [1] and the United States [2] have implemented targets for blending significant amounts of biofuels, on the order of 10% and greater, into the traditional fuel supply over the course of the next ten years. This requirement necessitates the development of new biofuel technologies through the conversion of lignocellulosic biomass [3]. Since the demand for diesel exceeded that for gasoline by 15% in 2009, and the growth in demand for diesel is expected to outpace that of gasoline by at least a factor of two through 2030 [4], there is a growing incentive to identify strategies for converting biomass to diesel. While biodiesel can be produced by transesterification of palm, rapeseed, or soybean oil, the supply of these oils is limited and is in demand for human nutritional use. An alternative approach that has received some attention is the synthesis of furanyl ethers [5–8]. Such ethers require little to no hydrogenation [9] and can be blended into petroleum-derived diesel up to 17 wt% with no adverse effects on engine performance and a decrease in particulate emissions [10] because of the high cetane number of ether groups [11].

An example of a furanyl ether is 5-(ethoxymethyl)furfural (EMF). The energy density of EMF is 30.3 MJ/L, almost 30% higher than that of ethanol and comparable to that of gasoline (31.1 MJ/L) [12]. One approach for producing EMF with high yields involves the formation of 5-(chloromethyl)furfural (CMF) as an intermediate by acid-catalyzed dehydration of sugars in a concentrated aqueous HCl and LiCl solution [12]. CMF will then react with ethanol to form EMF and HCl with 95% yield [13]. One concern with this approach is the separation and recycling of HCl. There are also substantial concerns about the introduction of unreacted chlorine-containing products into the automobile fuel delivery system and engine.

We have recently reported that EMF can be produced by acid-catalyzed etherification of HMF and ethanol [5]. The aim of the present study is to expand the scope of furanyl ethers that can be produced by this approach (Fig. 1) and to understand the mechanism and kinetics of such reactions. In the hydrogenolysis of HMF to 2,5-dimethylfuran (DMF), 5-(methyl)furfuryl alcohol (MFA) and 2,5-bis(hydroxymethyl)furan (BHMF) are formed as by-products [14]. These compounds can undergo etherification to form products that could be even more attractive than EMF as diesel blending agents because they do not contain aldehyde groups that are known to decrease the cetane number of diesel components [11]. A further goal of this study is to elucidate the mechanism and kinetics of furanyl ether formation with the aim of identifying

* Corresponding author.
E-mail addresses: Eric.Sacia@berkeley.edu (E.R. Sacia), Balki@berkeley.edu (M. Balakrishnan), bell@cchem.berkeley.edu (A.T. Bell).

http://dx.doi.org/10.1016/j.jcat.2014.02.012
0021-9517/

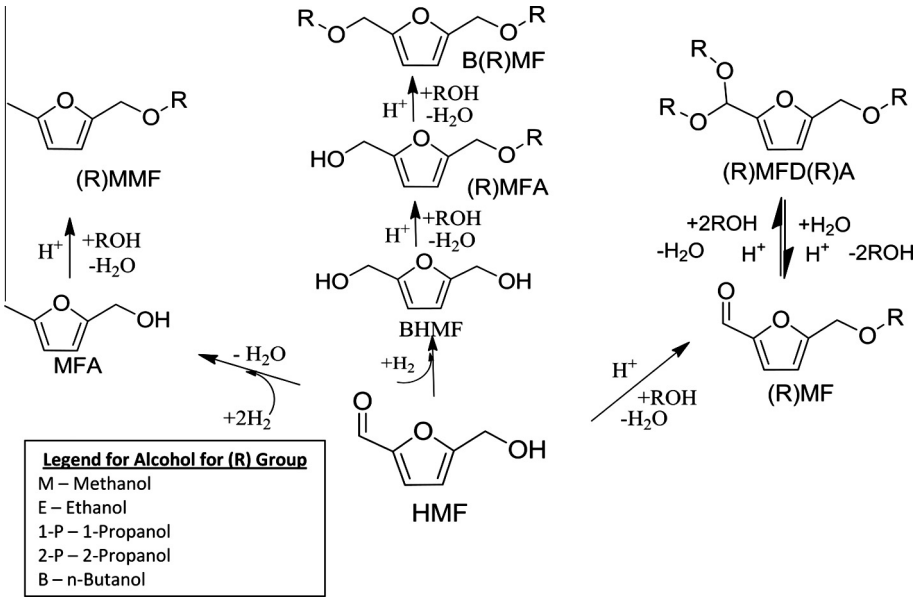

Fig. 1. Transformation of the HMF derived furanyl alcohols into fuel candidate molecules.

conditions for maximizing the yield of these products and understanding the role of the catalyst in determining selectivity.

2. Materials and methods

2.1. Experimental materials

All chemicals were used as received. 5-(hydroxymethyl)furfural (HMF) was purchased from Sigma–Aldrich in >99% purity. Both Amberlyst™ 15 (A-15) and Nafion® SAC-13 were purchased from Sigma–Aldrich. Methanol, 1-propanol, and 2-propanol used for etherification were obtained from Fisher Scientific in >99% purity. Absolute ethanol was purchased from Acros Organics in >99.5% purity, while 1-butanol was purchased from Mallinckrodt Chemicals in >99.4% purity. Ethyl acetate and hexanes (HPLC Grade), used for dilution and reaction respectively, and anhydrous Na_2CO_3 and $NaHCO_3$, used for neutralization, were obtained from Fisher Scientific. N,O-bis(trimethylsilyl)trifluoroacetamide with 1% TMSCl was purchased from Acros Organics and was used for silylation of alcohols to enhance separation by gas chromatography.

The reactants MFA and BHMF were synthesized via sodium borohydride reduction of 5-(methyl)furfural and HMF, respectively, and were purified for use in standard techniques (see Supplemental information). Calibration standards for gas chromatography for the ethyl ethers of MFA, BHMF, and HMF were synthesized from experimentally determined reaction conditions and purified through column chromatography (see Supplemental information). The purity of the synthesized compounds was verified by GC and NMR.

2.2. Etherification reactions

The etherification of furanyl alcohols was typically carried out using 10–100 mM concentrations of the furanyl alcohol, 0.9–35.5 mol% acid, and either ethanol or butanol as the solvent. Reactions below the boiling point of the solvent were performed using magnetic stirring at 600 RPM in sealed scintillation vials on an IKA RCT Basic stir plate equipped with an IKA ETS-D5 temperature controller. Reactions at 0 °C were carried out in an ice bath with a thermocouple to monitor solution temperature. Reactions between 0 °C and 25 °C were carried out on a heated stir plate in a refrigerated cold room that was maintained at 4 °C. Etherification reactions for HMF occurred at temperatures above the boiling point of the solvent and were performed in sealed headspace vials equipped with a silicone rubber septum for online sampling. In the cases where online sampling was required, filtration of solid catalysts was performed *in situ* during sample removal by passage through a packed-cotton filter (see diagram in Supplemental information).

Solutions of reactants and inert internal standard were allowed to reach the desired reaction temperature prior to catalyst addition. If less than 4.0 mg of Amberlyst-15 was required or in all cases for HMF etherification, the catalyst was dispensed as a 5.00 mg/mL suspension in the alcohol in which the reaction was carried out. Otherwise, the catalyst was added directly to the reactor as a solid. Samples were removed after a specified reaction time. When soluble acids were used as the catalyst, the reaction mixture was neutralized with $NaHCO_3$ at the end of the reaction period. Heterogeneous catalysts were removed by filtration through a column packed with cotton, silica gel, and $NaHCO_3$ to neutralize protons liberated by ion exchange. Ethyl acetate was then used to wash filtration columns and dilute the solutions to the necessary concentrations for evaluation by gas chromatography.

2.3. Product analysis

Product analysis was carried out using a Varian CP-3800 gas chromatograph equipped with both a flame ionization detector (FID) and a Varian 320 triple quadrupole mass spectrometer (MS). Compounds analyzed were separated in both cases using a FactorFour capillary column (VF-5 ms, 30 m length, 0.25 mm diameter) coated with a 0.25 mm thick stationary phase (5% phenyl and 95% dimethylpolysiloxane). All quantification was performed using the FID detector to achieve high signal to noise, while product identification was performed by mass spectrometry. To maximize accuracy of quantification, dodecane was used as an internal standard to rectify errors caused by variability in sample size delivery and detector signal strength [15]. FID response factors for ethers other than the synthesized ethyl ethers were estimated using the effective carbon number method, which predicts FID response to within ±1.7% [15–17]. To achieve sufficient baseline separation of

ethyl ethers of HMF and BHMF, reaction products were silylated with N,O-bis(trimethylsilyl)trifluoroacetamide with 1% TMSCl at 70 °C for 1 h, providing consistent, baseline resolved peaks.

2.4. Isotopic exchange of ether group of EMMF

Deuterated ethanol (ethanol-1,1,2,2,2-d_5, 99.5% atom D) was purchased from Aldrich to measure ethyl ether exchange rates for 2-(ethoxymethyl)-5-methylfuran (EMMF). EMMF that was synthesized and purified by column chromatography was immersed in a solution of the deuterated ethanol at a concentration of 10 mM at 25 °C. A dispersion of A-15, ground and sieved to 38–53 μm, was added such that the solution averaged catalyst concentration was 0.09 mM. Samples were taken periodically, centrifuged to remove catalyst, and run on a Varian CP-3800 gas chromatograph with Varian 320 triple quadrupole mass spectrometer to assess rates of ethyl exchange.

2.5. ^{13}C NMR investigation of A-15

Interactions of alcohols with the active site of A-15 were investigated using inverse-gated, proton-decoupled ^{13}C NMR. Experiments were carried out on a Bruker AV-600 instrument using the zgig30 pulse program. Data analysis was performed using MNova 7 [18]. A typical experiment involved adding 0.50 g of a 50:50 (wt%) mixture of the alcohol and $CDCl_3$ to 0.20 g of either A-15 or Amberlite XAD-1180 N that had been dried overnight *in vacuo* at 65 °C. Signals were then acquired for 1000 scans. Ethanol and 2-furanethanol were used as probe molecules to measure surface interaction with A-15 at 25 °C. 2-furanethanol was synthesized and purified before use via Wittig olefination of furfural followed by hydroboration/oxidation. The full procedure is described in the Supplemental information.

3. Results and discussion

3.1. Catalyst selection

The etherification of MFA with ethanol was chosen to evaluate the effectiveness of different acid catalysts. Trifluoroacetic acid, *p*-toluenesulfonic acid (*p*-TSA), sulfuric acid, and triflic acid were used as soluble acids for the reaction of MFA with ethanol to form 2-(ethoxymethyl)-5-methylfuran (EMMF) (Scheme 1). While the rate of EMMF formation varied with the extent of acid dissociation [19], the selectivity toward EMMF was independent of acid composition, 61.5% ± 5.4% (Table 1). The yield of EMMF was slightly lower in the case of triflic acid because the high acid strength resulted in increased decomposition of EMMF. The similarity in selectivity of different homogenous acids suggests that the etherification of MFA occurs via general acid catalysis in homogeneous solutions.

Several heterogeneous acids were explored in an attempt to maximize the yield of desired products through specific acid catalysis while also increasing the ease of catalyst recyclability. Brønsted acidic zeolites were considered because of their high surface areas and known shape selectivity [20,21]. As can be seen in Table 1, H-FAU had a lower selectivity than H-MFI, presumably due to its large supercage structure which more readily allows the formation of larger oligomers of MFA. Since zeolites were observed to deactivate due to oligomer formation and consequent plugging of the catalyst pores, these catalysts were not investigated further.

High product selectivity could be achieved with Nafion SAC-13, a dispersion of a sulfonated tetrafluoroethylene based fluorocopolymer over high surface area silica (Table 1, entry 6); however, this material also slightly deactivated with time. Near quantitative conversion of MFA to EMMF was achieved with Amberlyst-15 (A-15), a sulfonated polystyrene resin with a high density of acid sites (4.7 mol/kg) and large pores (30 nm) [22–23]. Moreover, this catalyst could be recycled a number of times without a loss in activity (see Supplemental information). Due to its exceptional reactivity and selectivity, A-15 was chosen as an appropriate catalyst with which to perform the remainder of the studies reported here.

To assess the extent to which intraparticle mass transfer affects the activity of A-15, experiments were conducted with particles of progressively smaller diameter. Table 2 shows that as the diameter was reduced from 600–800 μm to <38 μm, the activity per proton increased 6.6-fold. Since particles of the smallest three size ranges exhibited activity within 6% of the mean, the smallest particles of a defined size range, 38–53 μm, were used for measurements of reaction kinetics. A calculation of the Thiele parameter was carried out in order to further confirm the absence of intraparticle mass transfer effects. The Wilke–Chang correlation was used to estimate the effective diffusivity at 25 °C and the method of Le Bas was used to estimate the molecular volume of MFA at the normal boiling point [24]. From these estimates, the Thiele modulus, φ, was

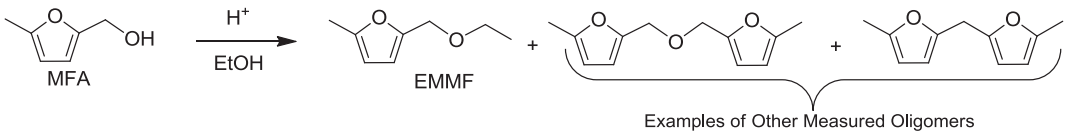

Scheme 1. Acid catalyzed etherification of MFA in an ethanol solution shown with presence of other oligomers.

Table 1
Screening of solid and soluble acids for the etherification of MFA to EMMF.

Entry	Acid catalyst	Reaction time (min)	MFA conversion (%)	EMMF yield (%)	EMMF selectivity (%)
1	p-TSA	120	94.3	60.0	63.6
2	Sulfuric acid	120	97.1	63.7	65.6
3	Triflic acid	60	100.0	55.4	55.4
4	H-FAU	120	81.9	64.6	78.9
5	H-MFI	120	48.1	42.8	89.0
6	Nafion SAC-13	120	89.8	83.1	92.5
7	A-15	120	99.7	>98%	>98%

In all experiments, starting materials were mixed, added to a heating plate at 25 °C, stirred at 600 RPM, and vials were removed and the acid was neutralized at indicated time points. Conditions: Entry 1–3 – MFA (83.3 mM), 35.5 μmol acid (35.5 mol%), 1.2 mL ethanol; Entry 4–5 – MFA (83.3 mM), zeolite (Si/Al = 15) 17.7 μmol acid sites (35.5 mol% acid sites), 0.6 mL ethanol; Entry 6 – MFA (83.3 mM), 35.5 μmol acid sites on SAC-13 (35.5 mol% acid sites given previously measured acid loading [31]), 1.2 mL ethanol; Entry 7 – MFA (83.3 mM), 35.5 μmol acid sites on A-15 (35.5 mol% acid sites), 1.2 mL ethanol.

Table 2
Effect of particle size on the rate of MFA etherification catalyzed by A-15.

A-15 particle size (diameter – μm)	Initial TOF (h^{-1})
600–800	0.29
75–125	1.39
53–75	1.66
38–53	1.72
<38	1.85

Reaction conditions: 25 °C, 10 mM MFA, 35.5 μmol acid sites on A-15, 10 mL ethanol.

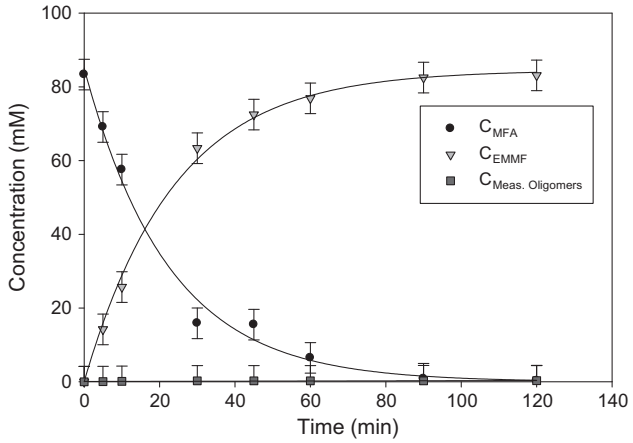

Fig. 2. Time course study of MFA etherification in ethanol. Conditions: 25 °C, 83.3 mM MFA, 1.2 mL EtOH, 35.5 μmol active sites on A-15 (as received).

determined to be 0.37 for particles in the range of sizes used (38–53 μm). A Thiele modulus of less than one confirms that all measurements of reaction kinetics were made in the reaction rate-limited regime.

3.2. Etherification of MFA with Amberlyst-15

3.2.1. Kinetics of etherification

The kinetics of MFA etherification with ethanol was measured in order to determine the reaction orders with respect to reactants and the dependence of the reaction rate on temperature. The reaction was zero order in concentrations of ethanol and water over the ranges tested, whereas the reaction was nearly first order (0.92 ± 0.1) in the concentration of acid sites and MFA (0.95 ± 0.1). An example of the temporal evolution of the product is given in Fig. 2, and a plot of the initial rate of MFA etherification as a function of reactant and catalyst concentrations is presented in the Supplemental information.

Due to the position of the hydroxyl group on the carbon adjacent to the aryl ring of MFA, the reaction should proceed through an S_N1 mechanism, as shown in Scheme 2. Water formed by protonation of the alcohol acts as the leaving group. Since the primary carbocation formed is unstable, the intermediate rearranges to form the more stable oxonium ion, as shown in step (2) of Scheme 2. The absence of diethyl ether from the products is attributed to the instability of the primary carbocation that would be necessary to form this product at the temperatures used in this study. The kinetics of this reaction was modeled using the Helfferich approach, a method often used to describe liquid-phase catalysis with polymeric resin catalysts, such as A-15, in the absence of transport limitations [25]. In this approach, the liquid–solid interaction is treated as a pseudo-homogeneous process since the reaction occurs in the solvation shell of the site. Assuming that the second step in Scheme 2 is the rate-limiting step, as is commonly the case for S_N1 reactions of this type [19], the following rate expression can be written:

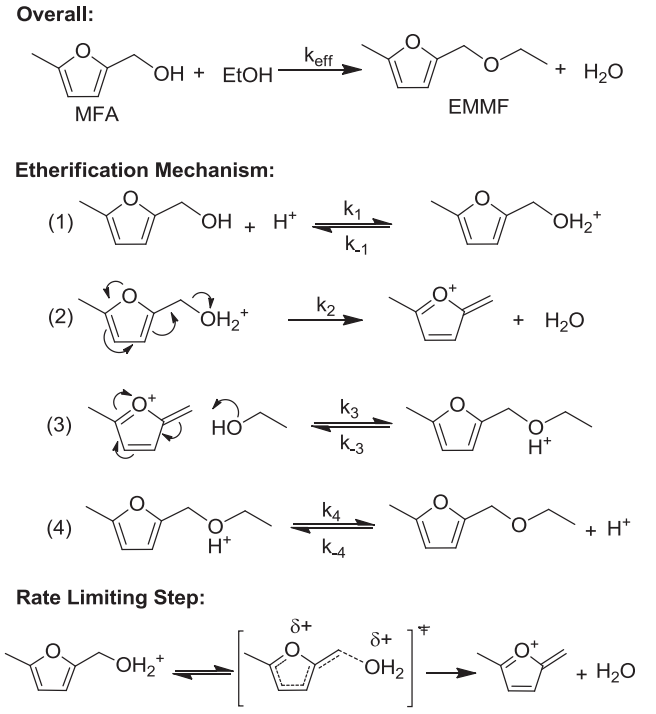

Scheme 2. Proposed mechanism for etherification of MFA with ethanol.

$$\frac{dC_{EMMF}}{dt} = r_{EMMF} = TOF_{EMMF} \times C_{H^+} = \frac{k_1 k_2}{k_{-1} + k_2} C_{H^+} C_{MFA} = k_{eff} C_{H^+} C_{MFA} \quad (1)$$

Since the rate of equilibration is much larger than the rate-limiting step, the equation for the turnover frequency (TOF) may be simplified as:

$$TOF_{EMMF} = K_1 k_2 C_{MFA} = k_{eff} C_{MFA} \quad (2)$$

In Eq. (2), $K_1 = k_1/k_{-1}$.

The observations reported above indicate that a pseudo-homogeneous model provides a satisfactory description of the intrinsic reaction kinetics. Further, it has been shown previously that, in the absence of diffusion limitations, the reaction rate order in the heterogeneous system matches that of the homogeneous system for resin catalysts [25]. For this reason, the reaction is treated as occurring at the liquid–solid interface of the cationic resin catalysts in which polar species are enriched in the strongly acidic phase near the surface [23,25–26].

Values of k_{eff} were determined by linear least squares regression of the initial rate of furanyl ether formation measured at low MFA conversion (<10%) and are listed in Table 3 for ethanol and butanol. The activation energies for MFA etherification in ethanol and 1-butanol were determined from Arrhenius plots (see Supplemental information). The apparent activation energy for etherification of MFA with ethanol is 17.0 ± 0.6 kcal/mol and that for etherification with 1-butanol is 19.9 ± 1.0 kcal/mol (Table 4).

The degree to which the formation of EMMF is reversible (see steps (3) and (4) of Scheme 2) was tested using isotopically labeled ethanol-1,1,2,2,2-d_5. The steps by which this reaction is thought to occur are shown in Scheme 3. Ethanol deuterium-labeled at all but the alcoholic hydrogen was used to prevent kinetic isotope effects from affecting the observed exchange rate. The rate at which the isotopic exchange occurred at 298 K was determined

by monitoring the intensities at m/z 140 and 145 (EMMF and EMMF-d_5, respectively). These experiments were carried out using molar concentrations of EMMF representative of those occurring in the measurements of the etherification of MFA. A plot displaying the initial exchange rate can be found in the Supplemental information. The ratio of the rate of MFA etherification over the rate of isotopic exchange at 25 °C is as follows:

$$\frac{TOF_{EMMF}}{TOF_{EMMF,exch}} = 101 \quad (3)$$

where TOF_{EMMF} is the initial turnover frequency of EMMF formation and $TOF_{EMMF,exch}$ is the initial exchange rate of the deuterated ether group. The much lower rate of ether exchange compared to the initial rate of MFA etherification is attributable to the lower pK_a of protonated ethers compared to alcohols [19], making the ether more difficult to protonate, and the decreased polarity of EMMF compared to MFA, making partitioning into the polar surface solvation shell more difficult.

3.2.2. The effect of A-15 on etherification selectivity

We hypothesize that, in the absence of pore-size constraints, the high EMMF selectivity of A-15 is due to decreased partitioning of the less polar furanyl alcohol compared to the more polar solvent alcohol into the solvation shell of A-15's acid sites. This idea is illustrated in Fig. 3. Once a furanyl alcohol molecule enters this acidic surface phase, it can react to form the oxonium ion and subsequently reacts with an ethanol molecule (Fig. 3c) to produce EMMF. It is well understood for S_N1 reactions that, once the cation is formed, the intermediate is relatively unselective with respect to the nucleophilicity of the nucleophile during step 3 in Scheme 2 [19]. By increasing the ratio of the solvent alcohol (ethanol of butanol) with respect to the furanyl alcohol in the phase around the site, reactions forming crossed ethers are favored over self-coupling of furanyl alcohols. The effects of this phenomenon become apparent when equimolar quantities of methanol, ethanol, 1-propanol, 2-propanol, and 1-butanol were added to a hexane solution. As supported by the data given in Table 5, the smaller, more polar alcohols react at higher rates with MFA than the larger, less polar alcohols.

To confirm the role of surface partitioning as a governing factor controlling selectivity, the surface phase of the catalyst was probed using inverse-gated, proton-decoupled ^{13}C NMR. Fig. 4 displays the position of the alcoholic carbon peaks of ethanol and 2-furanethanol. 2-Furanethanol was used as a proxy for MFA due to its similar size and polarity; however, it also exhibits limited reactivity due to the presence of an additional carbon atom between the alcohol group and the ring. The additional carbon prevents primary carbocation rearrangement and leads to relative inactivity over the time period of NMR measurement.

The spectrum of ethanol adsorbed in the pores of Amberlite XAD-1180N, a cross-linked polystyrene divinylbenzene copolymer analogous to A-15 but not containing sulfonic acid groups, is shown in spectrum A of Fig. 4. A single NMR peak is observed at 57.4 ppm corresponding to the methylene unit in a bulk chemical environment. The absence of a shift in the position of this peak relative to that for bulk ethanol indicates that the ethanol in the pores of Amberlite XAD-1180N interacts weakly with the unfunctionalized pore environment. By contrast, the spectrum of ethanol adsorbed into A-15 (spectrum B) exhibits a peak at 57.4 ppm for bulk ethanol and a second peak at 58.4 ppm corresponding to ethanol in exchange with the acid sites of A-15 over the timescale of NMR relaxation. Interaction with the acidic proton of A-15 leads to deshielding of the alcoholic carbon and a corresponding shift downfield for the second peak. The Bloch–McConnell equations can be used to describe the chemical exchange between the bulk and the first coordination sphere that is observed over the NMR timescale [27,28]. Relative peak intensities were obtained using a deconvolution algorithm for fitting Lorentzian peaks contained in MNova 7 [18]. The significant size of the peak at 58.4 ppm indicates that a large fraction of ethanol molecules have diffused through the bulk and undergone an equilibrated exchange with the surface over the course of the NMR relaxation time.

Similar to what is observed for ethanol, the alcoholic carbon of 2-furanethanol in the pores of Amberlite XAD-1180N displays a single peak located at 60.3 ppm (Fig. 4, spectrum C). When 2-furanethanol is mixed with A-15, a splitting similar to that seen for ethanol is observed (spectrum D), with the peak for the bulk alcohol appearing at 60.3 ppm and the peak for surface-exchanged alcohol appearing at 60.6 ppm. The spectrum obtained upon addition of a 25:25:50 (wt%) mixture of 2-furanethanol, ethanol, and $CDCl_3$ to A-15 is given in spectrum E. Disappearance of the surface peak for 2-furanethanol while both ethanol peaks remain indicates that ethanol outcompetes 2-furanethanol for interaction with the acidic site as a consequence of its smaller size and significantly higher polarity.

The results of our NMR studies are consistent with the picture presented in Fig. 3 and confirm that the alkyl alcohols are adsorbed preferentially into the pores of A-15. A direct consequence of the preferred adsorption of the alkyl alcohols is the high selectivity for forming EMMF, as shown in Fig. 2. A loss in EMMF selectivity does occur as the concentration of MFA in ethanol is raised; how-

Table 4
Apparent activation energies for MFA, BHMF, and HMF etherification with ethanol and butanol.

Furanyl alcohol	E_{app} (kcal/mol)		Pre-exp. factor (M^{-1}/min)	
	Ethanol	Butanol	Ethanol	Butanol
MFA	17.0 ± 0.6	19.9 ± 1.0	3.53×10^{13}	4.96×10^{16}
BHMF (1st ether)	18.1 ± 0.8	18.6 ± 1.6	1.48×10^{13}	7.45×10^{14}
BHMF (2nd ether)	20.0 ± 1.4	19.3 ± 0.9	3.49×10^{13}	4.78×10^{13}
HMF	25.7 ± 2.5	26.3 ± 1.5	1.24×10^{16}	4.80×10^{16}

Table 3
Rate constants for etherification of MFA, BHMF, and HMF in ethanol and butanol.

MFA				BHMF								HMF			
Ethanol		Butanol		Ethanol				Butanol				Ethanol		Butanol	
T (K)	$k_{eff}^{(a)}$ (M^{-1}/min)	T (K)	$k_{eff}^{(a)}$ (M^{-1}/min)	T (K)	$k_{eff,1}^{(a)}$ (M^{-1}/min)	T (K)	$k_{eff,2}^{(b)}$ (M^{-1}/min)	T (K)	$k_{eff,1}^{(c)}$ (M^{-1}/min)	T (K)	$k_{eff,2}^{(c)}$ (M^{-1}/min)	T (K)	$k_{eff}^{(d)}$ (M^{-1}/min)	T (K)	$k_{eff}^{(d)}$ (M^{-1}/min)
273.2	0.86	273.2	5.92	313.2	3.20	314.2	0.41	300.2	22.6	300.2	0.42	353.2	1.50	333.2	0.27
298.2	14.0	280.6	13.0	323.2	9.1	323.2	1.18	305.2	34.5	305.2	0.69	358.2	2.24	339.8	0.55
305.7	24.6	286.7	32.3	333.2	19.8	333.2	3.1	313.2	66.4	313.2	1.76	363.2	4.84	346.5	1.09
313.2	45.4	293.5	72.3	343.2	41.5	343.2	6.0	321.2	179	321.2	3.31	368.2	7.58	353.2	2.68
												373.2	9.45		

Reaction conditions: (a) 10 mM MFA/BHMF, 10.0 mL EtOH/BuOH solvent, 0.90 μmol acid sites on A-15 (38–53 μm), (b) 10 mM BHMF, 10.0 mL EtOH solvent, 18 μmol acid sites on A-15 (38–53 μm), (c) 10 mM BHMF, 7.0 mL BuOH solvent, 7.0 μmol acid sites on A-15 (38–53 μm) and (d) 100 mM HMF, 50.0 mL EtOH/BuOH solvent, 0.11 mmol acid sites on A-15 (38–53 μm).

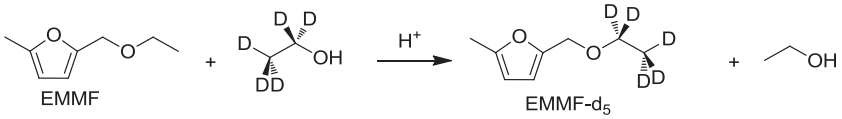

Scheme 3. Reaction performed during isotopic exchange of EMMF to measure reversibility of ether formation.

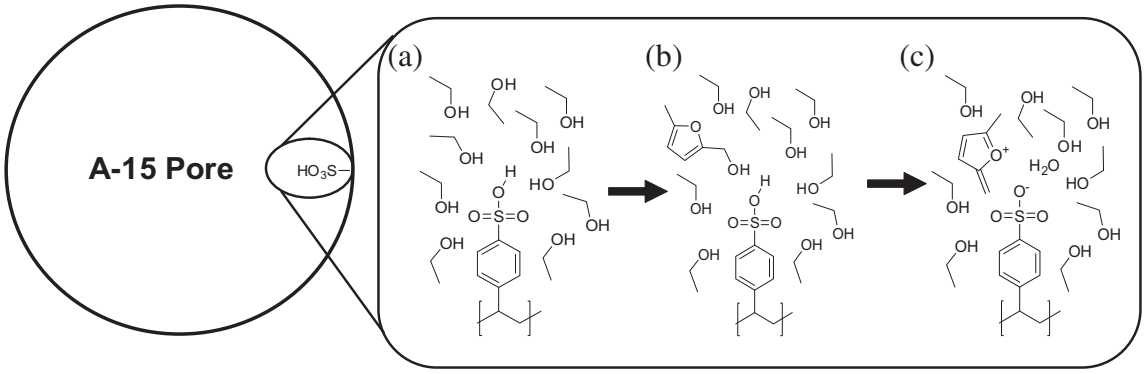

Fig. 3. Schematic of active site occupation during the course of reaction: (a) before furanyl alcohol enters acid solvation shell, (b) upon furanyl alcohol reaching surface acid sites and (c) upon formation of the reactive intermediate.

Table 5
Competitive reaction experiment forming various crossed ethers.

Alcohol incorporated into crossed ether	Initial TOF (h^{-1})
Methanol	1.12
Ethanol	0.93
1-Propanol	0.27
n-Butanol	0.12
2-Propanol	0.11

Reaction conditions: 25 °C, 10 mM MFA, 20 mM each alkyl alcohol, 0.90 μmol acid sites on A-15 (38–53 μm), 10.0 mL hexane as solvent.

ever, even a nearly eightfold increase in the concentration of MFA from 1.2 to 8.6 wt% only decreased the selectivity to EMMF from 98% to 84%.

3.3. Etherification of BHMF

The etherification of furanyl alcohols was extended to other C_6 furanyl alcohols, including HMF and BHMF. The products formed during the etherification of BHMF with ethanol are shown in Scheme 4. Fig. 5 shows that the formation of 5-(ethoxymethyl)furfuryl alcohol (EMFA) occurs much more rapidly than the subsequent etherification of EMFA to form 2,5-bis(ethoxymethyl)furan (BEMF). The second step, in which EMFA reacts to form BEMF, occurs nearly quantitatively, while the first step occurs with lower selectivity (~80%). The observed pattern in selectivity is likely attributable to the higher polarity of BHMF with respect to the single ether, EMFA, allowing BHMF to partition better into the surface phase of the catalyst and form increased amounts of undesired oligomers and side products. This hypothesis is further supported by the low relative rates of the second reaction of EMFA to BEMF despite similar amounts of electron donation to the ring for BHMF and EMFA.

The kinetics of the sequential etherification of BHMF is first order in acid and furanyl alcohol and zero order in ethanol and water. By analogy with the kinetics for the etherification of MFA, we assume that the protonation of BHMF and EMFA is close to being equilibrated and that the S_N1 formation of the oxonium cation is rate limiting. The rate of consumption of BHMF and the rates of formation of unidentifiable oligomer products, EMFA, and BEMF are then given by:

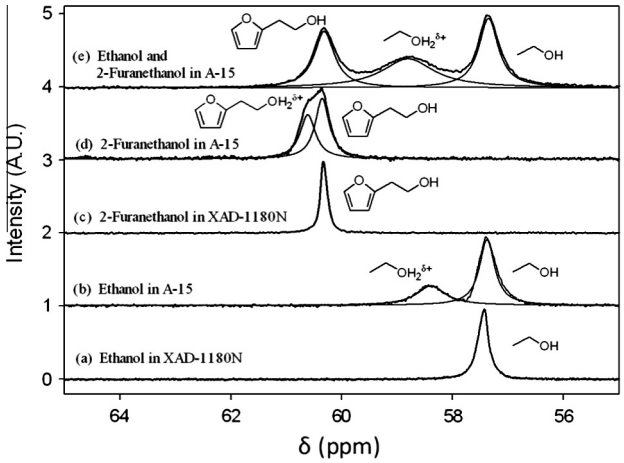

Fig. 4. ^{13}C NMR spectra of the alcoholic carbon of ethanol and 2-furanethanol in Amberlite XAD-1180N and A-15.

$$\frac{dC_{BHMF}}{dt} = r_{BHMF} = TOF_{BHMF} \times C_{H^+} = -k_{eff,1} C_{H^+} C_{BHMF} - k_U C_{H^+} C_{BHMF} \quad (4)$$

$$\frac{dC_U}{dt} = r_U = TOF_U \times C_{H^+} = k_U C_{H^+} C_{BHMF} \quad (5)$$

$$\frac{dC_{EMFA}}{dt} = r_{EMFA} = TOF_{EMFA} \times C_{H^+} = k_{eff,1} C_{H^+} C_{BHMF} - k_{eff,2} C_{H^+} C_{EMFA} \quad (6)$$

$$\frac{dC_{BEMF}}{dt} = r_{BEMF} = TOF_{BEMF} \times C_{H^+} = k_{eff,2} C_{H^+} C_{EMFA} \quad (7)$$

Solving Eqs. (4)–(7) results in the following expression for the temporal evolution of products:

$$C_{BHMF} = C_{BHMF,0} * e^{[-(k_{eff,1}+k_U)C_{H^+}*t]} \quad (8)$$

$$C_{EMFA} = \frac{k_{eff,1} C_{BHMF,0}}{k_{eff,2} - k_{eff,1} - k_U} * \left[e^{(-[k_{eff,1}+k_U]C_{H^+}*t)} - e^{(-k_{eff,2}C_{H^+}*t)}\right] \quad (9)$$

$$C_{BEMF} = \frac{k_{eff,1} C_{BHMF,0}}{k_{eff,2} - k_{eff,1} - k_U} * \left[e^{(-k_{eff,2}C_{H^+}*t)} + \frac{k_{eff,2}}{k_{eff,1} + k_U}\left(1 - e^{(-[k_{eff,1}+k_U]C_{H^+}*t)}\right) - 1\right] \quad (10)$$

$$C_U = \frac{k_U C_{BHMF,0}}{k_{eff,1} + k_U} * \left[1 - e^{(-[k_{eff,1}+k_U]C_{H^+}*t)}\right] \quad (11)$$

In Eqs. (8)–(11), $C_{BHMF,0}$ is the initial concentration of BHMF. Values for $k_{eff,1}$ and $k_{eff,2}$ were determined by a least-squares fit of Eqs. (8)–(11) to the data presented in Fig. 5 and are given in Table 3. The solid curves appearing in Fig. 5 were generated by plotting Eqs. (8)–(11) using the values of $k_{eff,1}$ and $k_{eff,2}$ listed in Table 3. The excellent fit of the model to the data is evident. Apparent activation energies for each etherification step were obtained from an Arrhenius plot of the natural log of $k_{eff,1}$ and $k_{eff,2}$ versus inverse temperature and are listed in Table 4. The results presented in Table 3 show that the etherification of BHMF proceeds at higher temperatures than the etherification of MFA. The latter compound is more reactive than the former because the electron-donating methyl group on MFA helps to stabilize the transition state for the rate-limiting step.

As mentioned previously, BHMF displays lower combined selectivity to EMFA and BEMF due to the high partitioning of BHMF into the solvation environment of the acid sites in A-15. Since S_N1 reactions tend to not be selective with regard to nucleophilicity [19], once the active oxonium ion is formed, a higher local concentration of the furanyl alcohol around the site will cause a decrease in the selectivity for crossed furanyl ethers. Therefore, there is a significant decrease in selectivity to desired products as the concentration of BHMF is increased. An increase in the concentration of BHMF from 1.3 to 9.7 wt% decreased the selectivity to BEMF from 79% to 53%.

3.4. Etherification of HMF

The temporal evolution of ether products formed during the etherification of HMF by ethanol at 80 °C is presented in Fig. 6. The etherified products can also react further to form ethyl levulinate and ethyl formate in stoichiometric ratios at long reaction times and high temperatures and acid loadings [5]. Due to the limited formation of these products over the timescales studied, the kinetics of their formation was not investigated.

While HMF can undergo direct etherification, acetalization of HMF prior to etherification is preferred in alcohol solutions (see Scheme 5). As discussed previously, the rate-limiting step in the etherification of furanyl alcohols involves the formation of an oxonium ion, and the reaction is facilitated at milder conditions by electron donation to the furan ring. Since HMF has an aldehyde group that is highly electron withdrawing due to the mesomeric effect [19], acetalization is preferred prior to etherification.

To test the validity of the reaction sequence shown in Scheme 5, the equilibrium in the first step was shifted from 5-(hydroxymethyl)furfural diethylacetal (HMFDEA) to HMF by the addition of water. The observed decrease in HMFDEA concentration led to a corresponding decrease in the rate of formation of etherified products (5-(ethoxymethyl)furfural diethylacetal (EMFDEA) and 5-(ethoxymethyl)furfural (EMF)), showing that HMFDEA is the active intermediate for etherification (see Supplemental information).

As shown in Fig. 6, equilibrium between the aldehyde and the acetal is established rapidly due to the significantly higher rate of acetalization compared to etherification. Therefore, the acetalization of HMF and EMF can be treated as quasi-equilibrated. The corresponding equilibrium constants K_α and K_β are defined by Eqs. (12) and (13):

$$K_\alpha = \frac{k_\alpha}{k_{-\alpha}} = \frac{C_{HMFD(R)A} C_{H_2O}}{C_{HMF} C_{ROH}^2} \quad (12)$$

$$K_\beta = \frac{k_\beta}{k_{-\beta}} = \frac{C_{(R)MF} C_{ROH}^2}{C_{(R)MFD(R)A} C_{H_2O}} \quad (13)$$

Values of K_α and K_β were determined at each data point by measuring the concentrations of furanyl alcohols and ethers. The concentrations of the furanyl alcohols and ethers were determined by GC and the amount of water was determined initially by Karl Fischer titration and by a material balance at subsequent data points. The values of K_α and K_β at each temperature were determined by averaging the measured values of the equilibrium constants found throughout the course of reaction. By this means, it was determined that, similar to the acetalization of benzaldehyde [29], formation of the acetal is exothermic, resulting in a higher concentration of aldehyde products with increasing temperature. The enthalpy of reaction for the equilibration of HMF with its dibutyl acetal, ΔH_α, is -16.0 ± 2.3 kJ/mol, and for the second equilibration step, ΔH_β,

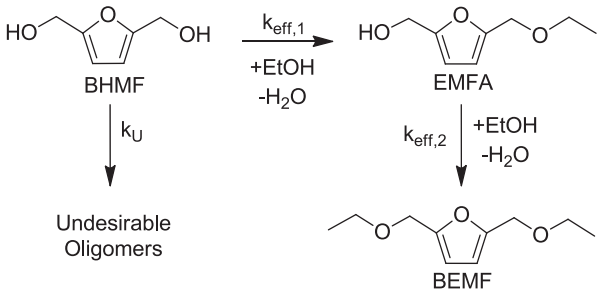

Scheme 4. Proposed pathway for BHMF etherification with ethanol.

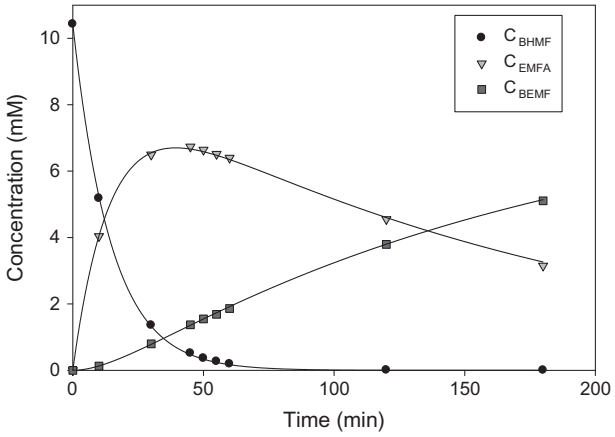

Fig. 5. Temporal product distribution during BHMF etherification with ethanol. Reaction conditions: 60 °C, 10 mM BHMF, 10.0 mL ethanol as solvent, 18 μmol acid sites on A-15 (38–53 μm).

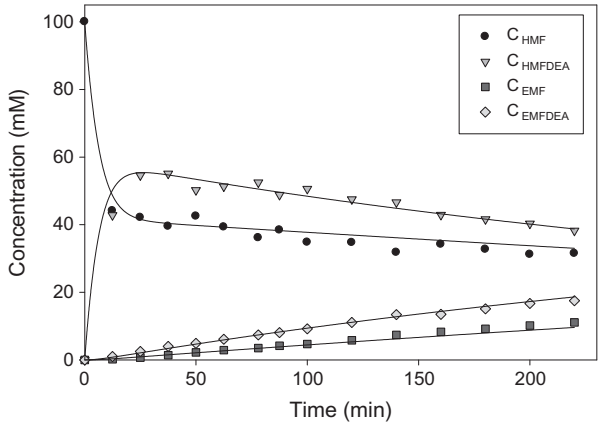

Fig. 6. Temporal product distribution during HMF etherification with ethanol. Reaction conditions: 80.0 °C, 100 mM HMF, 50.0 mL ethanol solvent, 0.11 mmol acid sites on A-15 (38–53 μm).

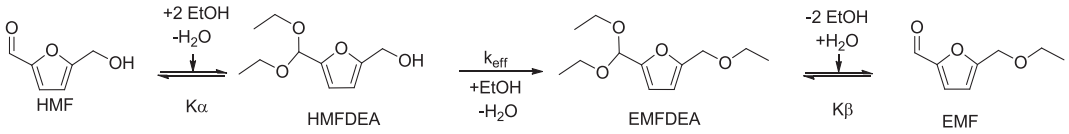

Scheme 5. Proposed pathway for HMF etherification with ethanol.

was determined to be 24.7 ± 6 kJ/mol during the etherification of HMF with butanol. Values for the equilibrium constants can be found in the Supplemental information.

As previously discussed, the etherification step was assumed to be first order in the concentration of the acid sites and the furanyl alcohol (HMFDEA in Scheme 5) and zero order with respect to ethanol and water concentration, giving the following rate expression:

$$-(\mathrm{TOF_{HMF}} + \mathrm{TOF_{HMFDEA}}) = (\mathrm{TOF_{EMF}} + \mathrm{TOF_{EMFDEA}}) = k_{\mathrm{eff}} C_{\mathrm{HMFDEA}} \quad (14)$$

The temporal dependence of the concentration of each component is then given by Eqs. (15)–(19) for any alcohol solvent:

$$\frac{dC_{\mathrm{HMF}}}{dt} = -k_{\alpha} C_{\mathrm{HMF}} C_{\mathrm{ROH}}^2 + k_{-\alpha} C_{\mathrm{HMFD(R)A}} C_{\mathrm{H_2O}} \quad (15)$$

$$\frac{dC_{\mathrm{HMFD(R)A}}}{dt} = k_{\alpha} C_{\mathrm{HMF}} C_{\mathrm{ROH}}^2 - k_{-\alpha} C_{\mathrm{HMFD(R)A}} C_{\mathrm{H_2O}} - k_{\mathrm{eff}} C_{\mathrm{H^+}} C_{\mathrm{HMFD(R)A}} \quad (16)$$

$$\frac{dC_{\mathrm{(R)MFD(R)A}}}{dt} = -k_{\beta} C_{\mathrm{(R)MFD(R)A}} C_{\mathrm{H_2O}} + k_{-\beta} C_{\mathrm{(R)MF}} C_{\mathrm{ROH}}^2 + k_{\mathrm{eff}} C_{\mathrm{H^+}} C_{\mathrm{HMFD(R)A}} \quad (17)$$

$$\frac{dC_{\mathrm{(R)MF}}}{dt} = k_{\beta} C_{\mathrm{(R)MFD(R)A}} C_{\mathrm{H_2O}} - k_{-\beta} C_{\mathrm{(R)MF}} C_{\mathrm{ROH}}^2 \quad (18)$$

$$\frac{dC_{\mathrm{H_2O}}}{dt} = k_{\alpha} C_{\mathrm{HMF}} C_{\mathrm{ROH}}^2 - k_{-\alpha} C_{\mathrm{HMFD(R)A}} C_{\mathrm{H_2O}} + k_{\mathrm{eff}} C_{\mathrm{H^+}} C_{\mathrm{HMFD(R)A}} - k_{\beta} C_{\mathrm{(R)MFD(R)A}} C_{\mathrm{H_2O}} + k_{-\beta} C_{\mathrm{(R)MF}} C_{\mathrm{ROH}}^2 \quad (19)$$

There was an insufficient number of data points at short reaction times to accurately obtain values for k_{α}, $k_{-\alpha}$, k_{β}, and $k_{-\beta}$ in the equilibration of acetals and aldehydes due to the high rate of acetalization on the timescale of etherification. Therefore, values of k_{α} and k_{β} were chosen such that the acetalization rate would be significantly faster than the rate of etherification, and values for $k_{-\alpha}$ and $k_{-\beta}$ were determined using Eqs. (12) and (13) and the measured equilibrium constants.

The effective rate coefficient for the etherification step, k_{eff}, was then determined by fitting the concentration profiles predicted by Eqs. (15)–(19) to the experimental data points for HMF etherification in ethanol and 1-butanol using least-squares regression. The curves through the data shown in Fig. 6 exemplify the quality of fit for our model of the kinetics. Measured values of k_{eff} and the activation energies for HMF etherification in ethanol and butanol are given in Tables 3 and 4, respectively, whereas the Arrhenius plots from which the activation energies were derived are shown in the Supplemental information.

Finally, the extent to which HMF selectivity to the desired EMF and EMFDEA products could be maintained was also explored. For HMF concentrations of 1.3 wt% in ethanol, the combined selectivity to ethyl ether products was 93% at 90% HMF conversion. By increasing the loading of HMF to 9.6 wt%, the selectivity decreased slightly to 83%.

3.5. Effects of solvent environment

To this point, we have explored the mechanism of furanyl alcohol etherification and the measured kinetic parameters in ethanol and butanol catalyzed by A-15 for several substituents on the furan ring. In order to further elucidate the role of the alcohol solvent on MFA, BHMF, and HMF etherification, the effect of the solvent on the rate of etherification was also investigated. Fig. 7 shows the rate

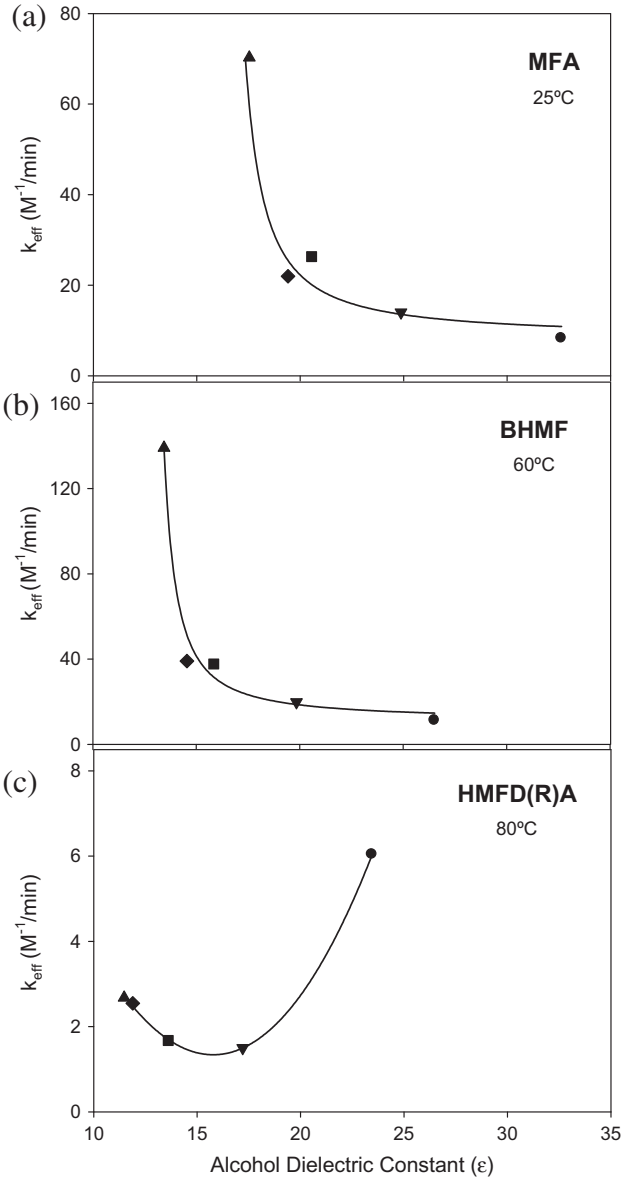

Fig. 7. Effects of solvent environment on rate of furanyl alcohol etherification for MFA, BHMF (first ether formation), and HMFD(R)A in methanol (●), ethanol (▼), 1-propanol (■), 2-propanol (♦), and 1-butanol (▲). Reaction conditions: (a) 25 °C, 10 mM MFA, 10.0 mL alcohol solvent, 0.90 μmol acid sites on A-15, (b) 60 °C, 10 mM BHMF, 10.0 mL ethanol as solvent, 0.90 μmol mM acid sites on A-15 and (c) 80 °C, 100 mM HMF, 50.0 mL alcohol as solvent, 0.11 mmol acid sites on A-15.

coefficient for each substrate as a function of the dielectric constant of the solvent. The dielectric constant of each solvent was determined at the corresponding reaction temperature using previously published values [30]. The solvent dielectric constant is chosen as a descriptor because it is known that for S_N1 reactions involving a neutral leaving group, increasing solvent polarity (viz., dielectric constant) decreases the rate of reaction [19]. This trend is a consequence of the fact that the positive charge is originally highly localized on the protonated alcohol intermediate, shown in step (2) of Scheme 2. The transition state for the release of H_2O involves delocalization of the charge so that it is shared between the ring and the leaving group. A more polar solvent is better able to stabilize the reactants with respect to the transition state; therefore, the rate decreases with increasing solvent polarity. This effect is largely manifested in the intrinsic rate constant (k_2 of Eq. (2)). Since the furanyl alcohol will also more readily partition into a less polar solvation shell containing butanol than one containing methanol, the effect of solvent polarity on reaction rate is further enhanced.

For MFA and BHMF etherification, the effect of changes in solvent polarity on rate is very similar. For HMF, acetalization precedes etherification, and the variation of the rate coefficient with dielectric constant is no longer monotonic. During the etherification of HMF in methanol, the active species undergoing etherification is the dimethyl acetal of HMF. Likewise, for etherification of HMF in butanol, it is the dibutyl acetal of HMF that undergoes etherification. Therefore, the observed dependence on dielectric constant can be attributed to competing effects between solvent polarity, which increases the intrinsic rate constant for the larger alcohols, and the "bulkiness" of the non-polar acetal group, which affects the partitioning of HMFD(R)A to the acid site's solvation shell. The highly non-polar acetal that is formed for the larger alcohols, like butanol, prevents partitioning and proper orientation into the solvation shell of the A-15 resin. Since the methoxy groups of the acetal in the methanol solvent are less bulky and more polar than their butoxy counterparts in butanol, the intermediate can better reach the acid site. Therefore, the competition between solvent polarity and the size of the acetal intermediate causes the trend observed in Fig. 7c.

4. Conclusions

Amberlyst-15 has been identified to be a highly active and selective catalyst for the etherification of MFA, BHMF, and HMF by C_1–C_4 alcohols. High selectivity to crossed ethers is achieved through the formation of a solvation shell of polar C_1–C_4 alcohols formed around the active site of the catalyst, as shown in Fig. 3. The proposed mechanism envisions that the oxonium ion formed in the rate-limiting step quickly reacts with a nearby nucleophile, such as ethanol. Due to the high relative abundance of the polar alcohol solvent in the solvation shell of the acid, crossed ethers are formed with high selectivity rather than undesired oligomerization of furanyl alcohols. The polarity of the alcohol around the acid site can also have a significant effect on the rate of etherification. Decreasing the solvent polarity increases the rate of product formation by nearly an order of magnitude, as was noted when methanol was replaced by 1-butanol as the solvent for MFA and BHMF etherification.

Systematic investigation of the etherification of C_6 furanyl alcohols demonstrates that the degree to which the substituents at the 2/5 position of the ring withdraw electron density from the ring strongly affects the rate of etherification. Since the methyl group of MFA donates electron density to the furan ring, the reactive oxonium intermediate is formed more readily and, correspondingly, the activation energy is lower than that observed for electron-withdrawing substituents. Progressing from BHMF to HMF, the ring substituent at the 2 position becomes more electron withdrawing. Since the aldehyde functionality of HMF is electron withdrawing due to resonance and inductive effects, the acetal is formed prior to etherification in alcohol solutions with A-15. The acetal, however, still causes the observed activation barrier for the etherification of HMF to be higher than that for etherification of BHMF or MFA. The mechanism of acetal formation proposed for HMF explains why this compound forms ethers at mild conditions in alcoholic solvents.

Acknowledgments

This work was funded by the Energy Biosciences Institute.This material is also based upon work supported by the National Science Foundation Graduate Research Fellowship under Grant No. DGE 1106400. The authors would also like to acknowledge the contributions of Taeryong Kim and Matthew Deaner for the experimental portion of this manuscript.

Appendix A. Supplementary material

Supplementary data associated with this article can be found, in the online version, at http://dx.doi.org/10.1016/j.jcat.2014.02.012.

References

[1] Renewable Energy Road Map, Renewable Energies in the 21st Century: Building A More Sustainable Future, COM(2006) 848 Final, Brussels, 2007.
[2] J.R. Regalbuto, Cellulosic biofuels—got gasoline?, Science 325 (2009) 822–824
[3] C. Somerville, H. Youngs, C. Taylor, S.C. Davis, S.P. Long, Feedstocks for lignocellulosic biofuels, Science 329 (2010) 790–792.
[4] F.S. Namat Abu Al-Soof, Brahim Aklil, Mohammad Taeb, Mohammad Khesali, Mohammad Mazraati, Benny Lubiantara, Taher Najah, Amal Alawami, Claude Clemenz, Nadir Guerer, Garry Brennand, Jan Ban, Joerg Spitzy, Douglas Linton, James Griffin, Martin Tallett, Petr Steiner, Ula Szalkowska, in: J. Griffin (Ed.), World Oil Outlook 2010, Organization of the Petroleum Exporting Countries, Vienna, Austria, 2010.
[5] M. Balakrishnan, E.R. Sacia, A.T. Bell, Etherification and reductive etherification of 5-(hydroxymethyl)furfural: 5-(alkoxymethyl)furfurals and 2,5-bis(alkoxymethyl)furans as potential bio-diesel candidates, Green Chem. 14 (2012) 1626–1634.
[6] L. Bing, Z. Zhang, K. Deng, Efficient one-pot synthesis of 5-(ethoxymethyl)furfural from fructose catalyzed by a novel solid catalyst, Ind. Eng. Chem. Res. 51 (2012) 15331–15336.
[7] L. Hu, G. Zhao, W. Hao, X. Tang, Y. Sun, L. Lin, S. Liu, Catalytic conversion of biomass-derived carbohydrates into fuels and chemicals via furanic aldehydes, Roy. Soc. Chem. Adv. 2 (2012) 11184–11206.
[8] B. Liu, Z. Zhang, One-pot conversion of carbohydrates into 5-ethoxymethylfurfural and ethyl D-glucopyranoside in ethanol catalyzed by a silica supported sulfonic acid catalyst, Roy. Soc. Chem. Adv. 3 (2013) 12313–12319.
[9] E.-J. Ras, S. Maisuls, P. Haesakkers, G.-J. Gruter, G. Rothenberg, Selective hydrogenation of 5-ethoxymethylfurfural over alumina-supported heterogeneous catalysts, Adv. Synth. Catal. 351 (2009) 3175–3185.
[10] P. Imhof, A.S. Dias, E. de Jong, G.-J. Gruter, OA02 – Furanics: Versatile Molecules for Biofuels and Bulk Chemicals Applications, NAM Abstract, 2009.
[11] M.J. Murphy, J.E. Taylor, R.L. McCormick, in: NREL (Ed.), Compendium of Experimental Cetane Number Data, Golden, Colo., 2004.
[12] M. Mascal, E.B. Nikitin, Towards the efficient, total glycan utilization of biomass, ChemSusChem 2 (2009) 423–426.
[13] M. Mascal, Edward B. Nikitin, Direct, high-yield conversion of cellulose into biofuel, Angew. Chem. Int. Ed. 47 (2008) 7924–7926.
[14] M. Chidambaram, A.T. Bell, A two-step approach for the catalytic conversion of glucose to 2,5-dimethylfuran in ionic liquids, Green Chem. 12 (2010) 1253–1262.
[15] J.T. Scanlon, D.E. Willis, Calculation of flame ionization detector relative response factors using the effective carbon number concept, J. Chromatogr. Sci. 23 (1985) 333–340.
[16] A.D. Jorgensen, K.C. Picel, V.C. Stamoudis, Prediction of gas chromatography flame ionization detector response factors from molecular structures, Anal. Chem. 62 (1990) 683–689.
[17] T. Holm, Aspects of the mechanism of the flame ionization detector, J. Chromatogr. A 842 (1999) 221–227.
[18] MestReNova, Mestrelab Research, Santiago de Compostela, Spain, 2012.
[19] E.V. Anslyn, D.A. Dougherty, Modern Physical Organic Chemistry, University Science Books, Sausalito, California, 2006.

[20] R.Q. Snurr, A.T. Bell, D.N. Theodorou, Investigation of the dynamics of benzene in silicalite using transition-state theory, J. Phys. Chem. 98 (1994) 11948–11961.
[21] M.W. Anderson, J. Klinowski, Direct observation of shape selectivity in zeolite ZSM-5 by magic-angle-spinning NMR, Nature 339 (1989) 200–203.
[22] Rohm&Haas, Amberlyst 15DRY: Industrial Grade Strongly Acidic Catalyst, Technical Data Sheet, Dow Chemical Company, 2005.
[23] C. Buttersack, Accessibility and catalytic activity of sulfonic acid ion-exchange resins in different solvents, React. Polym. 10 (1989) 143–164.
[24] B.E. Poling, J.M. Prausnitz, J.P. O'Connell, The Properties of Gases and Liquids, McGraw-Hill, 2001.
[25] A. Chakrabarti, M.M. Sharma, Cationic ion exchange resins as catalyst, React. Polym. 20 (1993) 1–45.
[26] D. Fărcaşiu, A. Ghenciu, G. Marino, K.D. Rose, Strength of solid acids and acids in solution. Enhancement of acidity of centers on solid surfaces by anion stabilizing solvents and its consequence for catalysis, J. Am. Chem. Soc. 119 (1997) 11826–11831.
[27] H.M. Mcconnell, Reaction rates by nuclear magnetic resonance, J. Chem. Phys. 28 (1958) 430–431.
[28] T.J. Swift, R.E. Connick, Nmr-relaxation mechanisms of 017 in aqueous solutions of paramagnetic cations and lifetime of water molecules in first coordination sphere, J. Chem. Phys. 37 (1962) 307.
[29] M.R. Altıokka, H.L. Hoşgün, Kinetics of hydrolysis of benzaldehyde dimethyl acetal over Amberlite IR-120, Ind. Eng. Chem. Res. 46 (2007) 1058–1062.
[30] C. Wohlfahrt, Static dielectric constants of pure liquids and binary liquid mixtures, in: O. Madelung (Ed.), Landolt–Börnstein – Group IV Physical Chemistry: Numerical Data and Functional Relationships in Science and Technology, Springer-Verlag, Berlin, 1991.
[31] Y. Liu, E. Lotero, J.G. Goodwin Jr, A comparison of the esterification of acetic acid with methanol using heterogeneous versus homogeneous acid catalysis, J. Catal. 242 (2006) 278–286.